Analysis and Modeling of Near-Ground Wave Propagation in the Presence of Building Walls

Fikadu T Dagefu, *Student Member, IEEE*, and Kamal Sarabandi, *Fellow, IEEE*

***Abstract*—An efficient semi-analytic model for near-ground wave propagation in indoor scenarios is presented. For transceivers deployed in indoor environments on or near the ground, since RF wave propagation is dominated by Norton surface waves, these higher order waves and their interactions with building walls and other indoor obstacles have to be captured for accurate field calculations. Existing ray tracing routines which are commonly used for indoor field prediction, are inadequate for evaluating signal coverage of transceiver nodes very close to the ground (less than a wavelength above ground) since such routines neglect higher order surface waves. In addition, geometrical optics alone is inadequate to treat finite-size and possible irregular-shaped obstacles at low radio frequencies (VHF and lower UHF). Our approach for calculation of near-ground wave propagation and scattering is based on a hybrid physical optics and asymptotic expansion of dyadic Green's function for a half-space dielectric medium. Equivalence principle in conjunction with physical optics approximation is utilized to handle scattered field from building walls which are the dominant scatterers in indoor settings. Simulation results for various indoor propagation scenarios based on the new approach is validated by using both measurement results and full-wave numerical solvers.**

***Index Terms*—Indoor field prediction models, near-ground wave propagation.**

I. Introduction

ELECTROMAGNETIC field prediction models for indoor and urban environments have several applications including wireless channel characterization, radar through-wall imaging and distributed sensor networks for environmental and subsurface sensing [1], [2]. Through-wall imaging and detection techniques, which have applications in many areas including fire and earthquake rescue missions and security systems (detection of intruders), often require a fast and accurate forward model which takes into account scattering from indoor obstacles. Another application pertains to positioning and tracking of robotic platforms deployed in complex environments including urban and indoor scenarios for military applications to enhance tactical situational awareness. A specific example of this is assisting the aforementioned platform in high-resolution navigation. There are also other military applications including sensor networks deployed in the battlefield for communications between soldiers on the ground. Examples of such systems that researchers have been working on include the self-healing minefield (SHM) system sponsored by DARPA [3] which is an anti-vehicle landmine system that utilizes a networked communication among the various mines and the networked embedded systems technology (NEST) which is also a DARPA program intended to be deployed in various environments [4]. The antennas used in such systems are often very close to the ground. For example, the antenna height of the SHM system is 7 cm [5]. One of the main goals of this paper is to present an indoor wave propagation model that accurately captures the Norton surface waves that are dominant at low transceiver heights.

In the literature, various indoor field prediction models have been presented. Ray tracing routines are used as the primary methods to predict field coverage in indoor and urban settings [6]–[16]. In [17], a hybrid technique that combines a full-wave approach with ray tracing is developed. In [18], a path loss prediction model that utilizes a parabolic approximation of the Helmholtz equation is proposed. There are also various high-frequency techniques including the Geometrical theory of diffraction (GTD) and Uniform theory of diffraction (UTD) that are devised to include diffraction effects from edges and corners [19]–[21]. Geometrical optics alone does not take into account finiteness and possible irregularities of building walls and other indoor scatterers. This is because of the inherent assumption used when the Fresnel reflection and transmission coefficients are derived in which the building wall is treated as an infinite homogeneous dielectric slab.

Several researchers have focused on developing indoor field prediction models that are based on measurement results especially for lower frequency applications [22]–[28]. Although models based on measurement could give a more accurate estimate of the received field compared to ray tracing routines, the drawback of such models is the fact that they are site-specific and hence are not versatile. Also, developing a measurement-based model is expensive and does not provide insight into the various scattering mechanisms. Pure numerical solvers that are based on methods such as MoM, FEM, FDTD, etc. are usually not preferred due to the high computational cost resulting from the large size of realistic indoor propagation scenarios in terms of wavelength. These methods are limited to low frequencies and small building scenarios and require high-performance computers.

Manuscript received June 04, 2010; revised October 14, 2010; accepted January 15, 2011. Date of publication April 21, 2011; date of current version June 02, 2011. This work was supported by the U.S. Army Research Laboratory under contract W911NF and prepared through collaborative participation in the Microelectronics Center of Micro Autonomous Systems and Technology (MAST) Collaborative Technology Alliance (CTA).

The authors are with the Radiation Laboratory, Department of Electrical Engineering and Computer Science, The University of Michigan, Ann Arbor, MI 48109 USA (e-mail: fikadu@umich.edu; saraband@umich.edu).

Color versions of one or more of the figures in this paper are available online at http://ieeexplore.ieee.org.

Digital Object Identifier 10.1109/TAP.2011.2144555

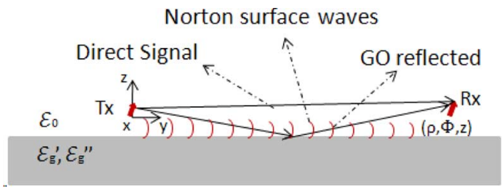

Fig. 1. A schematic of a near-ground Tx and Rx antennas on top of a dielectric half-space showing the direct, the GO-reflected and the Norton surface waves.

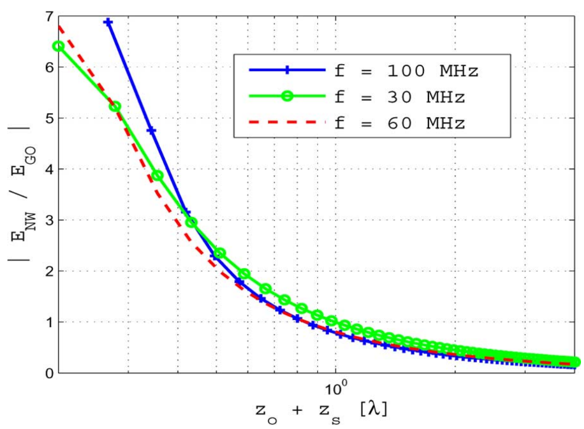

Fig. 2. The ratio of the higher order Norton surface waves contribution to GO component of the received field plotted against the height of the transceiver $(Rxh = Txh)$. The antennas are located above a half-space dielectric medium (as shown in Fig. 1), $\epsilon_{rg} = 4$ and $\sigma = 0.01$ S/m. The Tx antenna in this simulation is horizontally polarized.

Furthermore, the existing models including the various ray tracing and hybrid techniques are inadequate for evaluating the signal coverage for near-ground networks since the scattered wave from the ground is only approximated by using the Fresnel reflection coefficient neglecting the higher order surface waves. For near-ground transceivers, even without the presence of building walls, wave propagation is dominated by the Norton surface waves due to the near cancellation of the direct field with the GO reflected field (see Fig. 1), which are the first two terms in (1). The third term is particularly important at lower RF bands for *ad hoc* communication scenarios. The total electric field in the presence of the ground is given by

$$E_{total}^{No\ wall} = E_{direct} + E_{reflected}^{GO} + E_{\text{ground}}^{\text{Norton}}. \tag{1}$$

Since Norton waves vary as a function of the sum of the heights of the Tx and Rx antennas, the ratio of the Norton waves to the GO components $\left(E_{direct} + E_{reflected}^{GO}\right)$ is plotted against the sum of the transmitter height and receiver height $(zs + zo)$ in terms of wavelength as can be seen in Fig. 2. It should be noted that, $'zo + zs'$, shown in terms of wavelength (in the X axis), is calculated independently for each frequency. So, when the curve for the 30 MHz case is plotted, it's against the height in terms of wavelength at 30 MHz. The curves for the other frequencies are plotted in a similar fashion. As can be seen in the plot, the Norton waves are dominant independent of frequency as long as the transceiver height is small in terms of wavelength. The slight variation in the ratio (E_{NW}/E_{GO}) is caused by the change in the imaginary part of the dielectric constant as a function of frequency.

Based on the above analysis, we see that the higher order Norton waves and their interactions with building walls and other indoor obstacles have to be taken into account for accurate field calculation. Despite the extensive research that has been carried out recently in the area of indoor field prediction modeling, to our knowledge, an accurate and computationally efficient technique that fully takes into account these higher order Norton waves and can be applied for characterizing near-ground wave propagation especially in indoor scenarios is not available.

In this work, an efficient semi-analytic near-ground wave propagation model for indoor scenarios is proposed. The method is based on asymptotic behavior of dyadic Green's function for a half-space dielectric in conjunction with a physical optics approximation to handle scattered field from various indoor obstacles. Dielectric building walls, which are the most commonly encountered features in indoor and urban settings, are modeled as dielectric blocks whose effective dielectric constants are calculated based on the electromagnetic characteristics of the building materials. The field scattered by building walls and other indoor obstacles that are in the line of sight of the transmitter is computed by first approximating the total fields inside the dielectric medium using physical optics and then applying equivalence principle. The dielectric scatterers are then replaced by polarization currents which are used to calculate the first order scattered field. Geometric optics in conjunction with the Green's function is used to account for multiple reflections from the shadowed walls up to any desired order.

In Section II, we describe the proposed approach and discuss how the various components of the electric field are calculated in 2D for a simple wall-ground geometry followed by the extension of the 2D model to 3D multiwall scenarios. In Section III, the implementation and validation of the proposed technique by using numerical solvers followed by the comparison of Norton waves and the scattered field component from furniture are discussed. Also in this section, time-domain analysis of the received field, which is useful to get an insight into the various scattering mechanisms, is presented. In the last part of Section III, the accuracy and computational efficiency of the proposed technique is compared to that of ray tracing and a full-wave solver. In Section IV, measurement results from controlled laboratory measurements are used to further investigate the accuracy of the proposed technique. In all the formulations and discussions to follow e^{iwt} time variation convention is assumed.

II. Semi-analytic Approach

In this section, an efficient semi-analytic approach to calculate the received electric field in an indoor setting where both the transmitting and receiving antennas are located in close proximity to the ground (less than a wavelength above ground) is presented. It should be noted that, even though the focus here is on near-ground transceiver nodes, the formulation is general and is valid for arbitrary transceiver node heights. We first briefly describe the derivation of the asymptotic computation of the Green's function followed by the description of the approach we pursued to calculate the various components of the received field for a case where the Tx and Rx antennas are located on

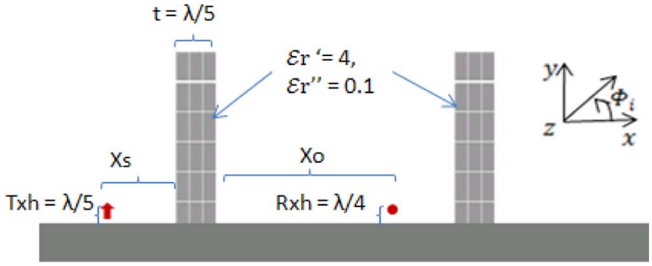

Fig. 3. A schematic showing the dielectric ground and building walls and a transmitting antenna and observation point.

either side of a single dielectric building wall. The extension of the method to multiwall scenarios will be discussed in the later part of this section.

A. Norton Surface Waves

The classic problem of calculation of the electric field radiated by an infinitesimal dipole located above a half-space medium has been investigated extensively [29]–[32]. The available solutions, however, involve the well known Sommerfeld integrals which are of the type given in (3) and are difficult to evaluate due the presence of poles and oscillatory properties of the integrals. Various exact and asymptotic solutions have been proposed to solve this issue. In [29], a method called the exact image theory is used to derive explicit expressions for fields radiated by dipoles above impedance surfaces. Asymptotic and ray tracing based approaches to efficiently calculate the field radiated by a dipole above a half-space and multilayer cases have also been proposed [30], [31].

For transceivers located in indoor scenarios, like the one shown in Fig. 3, the total electric field observed at the location of the receiver, can be decomposed into three components as given in the equation below. In the discussion below, the locations (in the rectangular coordinate system) of the Tx and Rx antennas is (x_s, y_s, z_s) and (x_o, y_o, z_o), respectively

$$E_{\text{total}} = E_{\text{direct}} + E_{\text{scattered}}^{\text{ground}} + E_{\text{scattered}}^{\text{walls}} \tag{2}$$

The first component is the field at the location of the receiving antenna if only the Tx and Rx antennas are present in free space. When the ground and the building walls are introduced, the second and third components are created, respectively. The field component scattered by the walls [the third term in (2)] includes both the reflected (or transmitted) component depending on where the receiver is located and diffracted components from the edges of the walls. Of course, the waves scattered by the ground, walls and other possible obstacles also interact with each other resulting in multiple scattering components. So, the scattered field components are not completely independent. As it was alluded to in the previous section, commonly used indoor field prediction techniques include the field component scattered by the ground by a first order approximation which includes the GO reflected field from the ground and the direct component neglecting the higher order Norton surface waves. In order to efficiently calculate the field coverage in indoor propagation scenarios, our approach utilizes a fast and accurate computation of dyadic Green's function for a half-space dielectric medium ($\overline{\overline{G}}_{00}$) as derived by Liao *et al.* [32].

The derivation of this solution begins with the twofold integral form of the dyadic Green's function which does not have a closed form solution [33]. After applying a change of variable, for the setup shown in Fig. 1, the scattered field from the ground at the location of the receiver (for $z_s > z_o$) can be written in terms of k_ρ (the component of the wave vector in the $\vec{\rho}$ direction in cylindrical coordinate system) and Bessel functions as given in (3), which involves the well-known Sommerfeld integral

$$E_{ij}^{\text{scattered}} = \frac{-\omega\mu_o I_o l_i}{8\pi} \int_0^\infty f_{ij}(k_\rho) e^{ik_{oz}(z_o+z_s)} d_{k_\rho} \tag{3}$$

In the above equation, the function f_{ij} is expressed in terms of k_ρ and Bessel functions. The indices i and j are the polarizations of the Tx and Rx antennas, respectively. $I_o\vec{I} = I_o(l_x\vec{x} + l_y\vec{x} + l_z\vec{z})$, ω and μ_o are the current moment vector, the angular frequency and free space permeability, respectively. The components of the wave vector (k_ρ and k_{oz}) are related by

$$k_o^2 = k_\rho^2 + k_{oz}^2. \tag{4}$$

After applying yet another change of variable in (3) for k_ρ ($k_\rho = k_o \sin\omega$), we use Hankel's functions to extend the limits of integration (from $-\infty$ to $+\infty$). The asymptotic forms of Hankel's functions for large arguments are then applied. Finally, the method of saddle point integration is used to get the saddle point contribution up to second order as given in

$$E_{ij}^{sp} = \frac{-k_o^3\eta_o I_o l_i}{8\pi} e^{ik_o\rho} \left[\frac{f_{ij}(w_s)}{ik_o\rho} + \frac{\frac{f_{ij}''(w_s)}{2} + \frac{f_{ij}(w_s)}{8}}{(ik_o\rho)^2} \right]. \tag{5}$$

As validated in the original work, it turns out that this contribution, when added to the direct signal, results in an accurate approximation of the received field in the presence of the ground. The first term in (5) is the Fresnel reflection contribution while the second term is known as Norton surface waves and become dominant when the transceiver height is small in terms of wavelength. The saddle point ($w = w_s$) is needed for the calculation of the saddle point contribution. Analytic expressions for f_{ij} are included in Appendix A. The saddle point is calculated using (R is the distance between the transmitter and receiver antennas)

$$\sin(w_s) = \frac{\rho}{R} \tag{6}$$

$$\cos(w_s) = \frac{z_o + z_s}{R} \tag{7}$$

$$R^2 = \rho^2 + (z_o - z_s)^2. \tag{8}$$

To get the total field components that make up the dyadic Green's function ($\overline{\overline{G}}_{00}$), the direct signal components have to be added to the scattered components discussed above. Finally, the dyadic Green's function can be written as

$$\overline{\overline{G}}_{00} = \frac{1}{jk\eta_o} \begin{bmatrix} E_{xx} & E_{yx} & E_{zx} \\ E_{xy} & E_{yy} & E_{zy} \\ E_{xz} & E_{yz} & E_{zz} \end{bmatrix}. \tag{9}$$

It should be noted that even if the derivation is for the case where the receiver is above the source $(z_s > z_o)$, the Green's function for the other case $(z_s < z_o)$ can be found by applying the principle of reciprocity which is mathematically equivalent to performing the complex transpose of the expression given in (9). This Green's function is used throughout the rest of the derivations. By making use of $\overline{\overline{G}}_{00}$ when calculating the wave radiated by the transmitting antenna, the background propagation medium is changed from free space to a half-space dielectric. This step enables us to include the first two components of the total field given in (2).

B. *Single Wall-Ground Geometry*

In this subsection, a way to efficiently calculate the field component scattered by indoor obstacles such as building walls, ceilings, and furniture [which is the third term in (2)] will be developed. The approach we pursued to calculate this component is by making use of physical optics approximation and volume equivalence principle in conjunction with the Green's function that was discussed. Let's first consider the problem geometry shown in Fig. 3 with a single dielectric building wall disregarding for now the second wall and any additional scatterers and discuss a way of calculating the scattered field by this wall. It should be noted that the field scattered by the building wall is computed in the presence of the ground. The extension of the method to a multiwall or more realistic indoor propagation scenarios will follow.

Volumetric polarization currents which will be used to replace the various dielectric scatterers are determined by the incident field from the transmitting antenna, boundary conditions on the wall surface and dielectric properties of the building wall. The effective dielectric properties of typical building walls such as brick or cinderblock can be measured or calculated based on available dielectric mixing models [36], [37]. Once the geometry and dielectric properties of the building walls are known, the first step is to calculate the incident electric field on the surface of the wall that is in the direct view of the transmitter. For a given antenna with known current distribution $\vec{J}$, the incident field on the wall surface can be calculated using

$$\vec{E}_{inc} = jk\eta_o \int\int\int \vec{J}(r')\overline{\overline{G}}_{00}(r,r')d_{r'}. \tag{10}$$

The incident field will then be decomposed into TE and TM components by using the following procedure:

$$\vec{E}_{inc}^{TM} = \vec{E}_{inc}\cdot\left(\frac{\vec{ki}\times\vec{n_w}}{|\vec{ki}\times\vec{n_w}|}\times\vec{ki}\right) \tag{11}$$

$$\vec{E}_{\rm inc}^{TE} = \vec{E}_{inc}\cdot\frac{\vec{ki}\times\vec{n_w}}{|\vec{ki}\times\vec{n_w}|}. \tag{12}$$

Here, $\vec{ki}$ is the unit vector in the direction of the incident field and $\vec{n_w}$ is the unit vector in the direction of the source and normal to the wall directly illuminated by the antenna. Once we have the TE and TM components of the incident field on the wall surface, we will then use them to approximate the fields inside the dielectric wall using physical optics approximation. The total field inside the wall is calculated locally assuming the wall is infinite and illuminated by a plane wave. It should be noted that this assumption will require that the Tx antenna be in the far-field region relative to the point in question inside the wall. The expressions for the total field inside the wall surface for the TE_z case are given in (13) and (14) below. Similar expressions can be found for the TM_z case by applying the principle of Duality.

$$E_x = \frac{-k_y}{\omega\epsilon_w}\left(A_w e^{ik_{wx}x} + B_w e^{-ik_{wx}x}\right)e^{ik_y y} \tag{13}$$

$$E_y = \frac{-k_{wx}}{\omega\epsilon_w}\left(A_w e^{ik_{wx}x} - B_w e^{-ik_{wx}x}\right)e^{ik_y y} \tag{14}$$

where k_{wi} $(i = x, y$ or $z)$ are the components of the propagation constant in the wall (k_w). A_w and B_w are

$$B_w = \frac{T_{TE}E_{inc}^{TE}}{1 - R_{TE}^2 e^{i2k_{wx}d}} \tag{15}$$

$$A_w = B_w R_{TE} e^{i2k_{wx}d} \tag{16}$$

$$T_{TM} = \frac{2k_{ox}\epsilon_{rw}}{k_{wx}\epsilon_o + k_{ox}\epsilon_{rw}} \tag{17}$$

$$R_{TM} = \frac{k_{wx}\epsilon_{ro} - k_{ox}\epsilon_{rw}}{k_{wx}\epsilon_{ro} + k_{ox}\epsilon_{rw}} \tag{18}$$

$$k_w^2 = k_{wx}^2 + k_{wy}^2 + k_{wz}^2 \& \quad k_w = w\sqrt{\mu\epsilon_w}. \tag{19}$$

In the above equations, d is the thickness of the wall. Having calculated the total fields inside the wall, we can obtain volumetric polarization currents based on the dielectric properties of the wall. The equation relating the total electric field inside the wall and the polarization current is

$$\vec{J}_{ep} = -iw\epsilon_o(\epsilon_{rw} - 1)\vec{E}. \tag{20}$$

The final step in calculating the scattered field by the building wall is to propagate the fields from the polarization currents using (10). Both the propagation from the source to the wall surface and the forward propagation of the field of the polarization currents to the observation point are calculated by taking the near-ground propagation effects into account. This method takes into account the Norton surface waves which affect the volumetric polarization currents of the wall and hence the scattered field by the building wall.

C. *Multiwall Scenarios*

For an indoor propagation scenario such as the setup shown in Fig. 4, the way the scattered field from each wall is calculated in the semi-analytic model is as follows: First the volumetric polarization currents for the walls in the direct view of the transmitter are computed by following the procedures outlined in Section II-B. Then, the field from these currents and the current on the transmitting antenna are computed using $\overline{\overline{G}}_{00}$ for any observation point within or outside the building. Finally, geometric optics is used to account for the shadowed walls. Basically near-ground fields from the source and the lit wall/s are reflected/transmitted at the specular points on the shadowed walls according to the Fresnel law of reflection and transmission to account for walls that are not in the direct view of the transmitter. This process can be followed multiple times to capture all multipath among the building walls. Since Norton waves decay very fast with propagation distance, one simplifying feature of

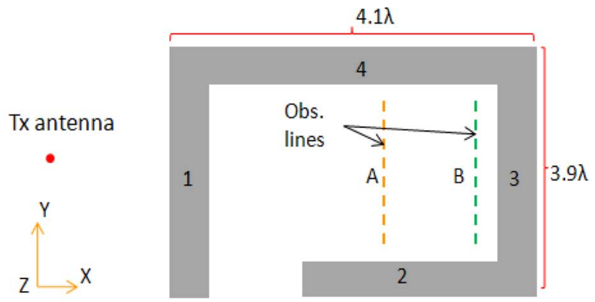

Fig. 4. A schematic (top view) of multiwall indoor propagation scenario showing the Tx antenna and the observation point (ground not shown).

near-ground propagation is that the convergence in field calculation is reached much faster than ordinary ray tracing. Simulations show that one or two iterations are sufficient to reach convergence. This approximation appears to be more accurate away from the edges of the walls and corners, as the near-field edge effects are not properly accounted for in our model.

III. Numerical Validation and Analysis

To validate the proposed hybrid model, a full-wave simulation is first used for the 2D wall-ground case. Numerical validation for a more complex indoor scenario in the 3D case is also presented. Time-domain analysis of the received field is performed in order to understand the various propagation mechanisms. Comparison of the scattered field component by a furniture against the contribution of Norton waves to the total electric field is presented. To assess the accuracy of the proposed technique as compared to ray tracing, error comparison against a ray tracing routine is discussed. Simulation results using a commercial FDTD solver is used as a reference in the error analysis. Also, the errors in the comparisons of the simulation results are explained by pointing out the various assumptions and approximations.

A. Validation of the 2D Single Wall-Ground Scenario

First, a single wall building geometry as shown in Fig. 3 (with one wall) in 2D where the length of the wall (along z direction) was assumed to have an infinite extent. As it is a 2D case, a line source of constant current with vertical polarization (y-directed) is used as a source which is placed 40λ away from the first wall. The observation point is varied on the other side of the wall along the X axis while keeping the height of the receiver the same. This scenario is simulated using both the proposed technique and a 2D numerical solver based on the Nystrom method [38].

The electric field calculated based on the two methods is plotted against the distances of the observation points from the first wall (denoted by Xo in Fig. 3). Two cases are considered where different heights of the transceivers is used. In the first case [shown in Fig. 5(a) and (b)], the heights of the transmitter and receiver are $z_s = 0.2\lambda$ and $z_o = 0.25\lambda$, respectively. In this case, the Tx and Rx heights are well within the height limits where the Norton waves become dominant as pointed out in Section II-A. In the second case [Fig. 5(c)], the Tx and Rx heights were increased to $z_s = 0.53\lambda$ and $z_o = 0.47\lambda$ in which case the Norton waves are still significant but not as dominant as the first case. In both cases, the dielectric constant for the wall and the ground is chosen to be $4+0.1j$ and the frequency is 200 MHz. The dielectric constants used for the wall and the ground are the same because of the limitations imposed by the numerical code we used for validation which was originally developed for simulation of propagation above rough surfaces [38].

For both scenarios, the components of the electric field computed using the proposed method show good agreements with that of the full-wave solution. However, there is about a maximum of 2 dB error and a slight shift in the maxima and minima where the errors are also higher. The discrepancies occur because of the approximations used both in the proposed semi-analytic technique and the full-wave solution. First, in the proposed technique, the calculation of the polarization currents for the dielectric wall is not exact. This is because when the total field inside the wall is computed, the wall is treated as an infinite dielectric slab which introduces an error in the total electric field inside the wall since the contributions to the field by any reflections from the wall edges are not accounted for. The second reason has to do with the accuracy of the full-wave model. To create the vertical wall structure, we are using a very large slope in the Nystrom model for dielectric surfaces. This creates inaccuracy in the calculated surface currents near the edges and corners. It should be noted that the error in the Nystrom approach is very small and this solution is discussed extensively and validated in the original work [38]. So, it makes sense to use it to validate our proposed approach. As seen in Fig. 5, the two independent methods are in good agreement.

B. How do Norton Waves and Scattering From Furniture Compare?

Having validated our proposed model for a single wall-ground geometry, we will proceed to show the significance of the Norton waves specifically for near-ground sensors in indoor scenarios. The careful reader might wonder how important taking the Norton waves into account is, specifically for indoor propagation environments. Here we will show that the Norton waves are actually more vital for accurate prediction of the electric field received by near-ground sensors than the inclusion of indoor obstacles such as furniture. To demonstrate this we carried out simulations to compare the Norton component to scattering from a wooden table. The setup of the simulation is given below.

In the first simulation, a horizontally polarized Tx antenna is positioned just above a half-space dielectric (as shown in Fig. 6) and the electric field at the location of the receiver is calculated for various points along the Z-axis. In the second simulation, we introduced a wooden table which we modeled by a thin homogeneous dielectric box and four cylindrically shaped dielectrics for the top part and the four legs, respectively. The dielectric constant of the table is assumed to be $\epsilon_{rg} = 1.4 + 0.0728j$. The dimensions of the table top is (2λ by 2λ by 0.1λ) and the each table leg is 1λ long having a diameter of 0.1λ. For this simulation d is chosen to be 25λ (Fig. 6). The table is positioned in the path of the direct signal from the Tx antenna to the Rx antenna so that the maximum effect of the table is included.

The scattered field from the table is calculated by using the Born approximation where the total field inside the dielectric

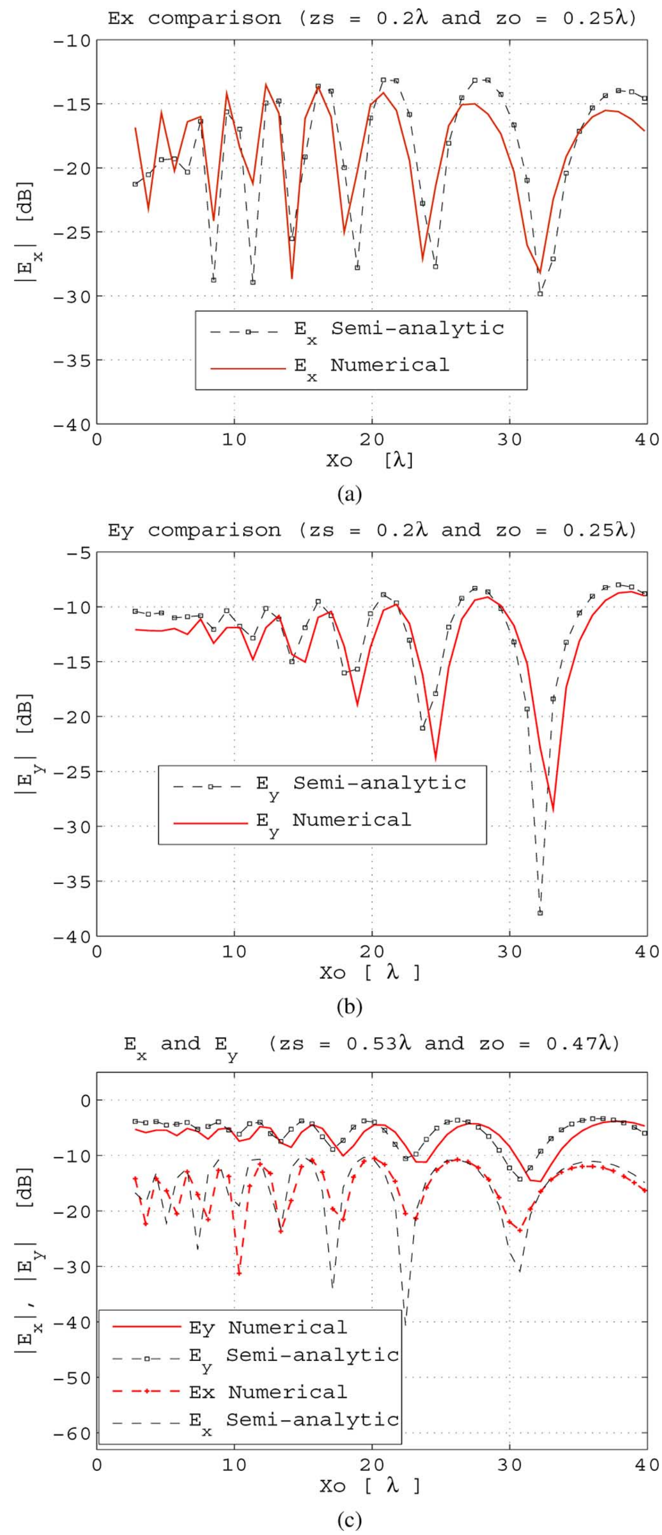

Fig. 5. Comparison of received electric for the single wall ground geometry (2D case) between the proposed technique and a numerical solution.

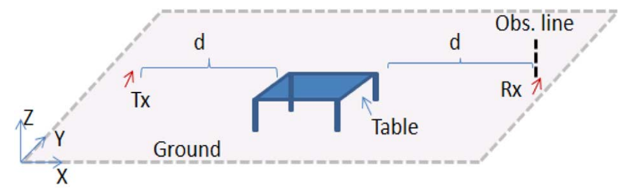

Fig. 6. Geometry used for the simulation for analysis of scattering from a wooden table. The dimensions of the table top is (2 m by 2 m by 0.1 m and each table leg is 1 m long having a diameter of 0.1 m. The frequency of simulation is 300 MHz.

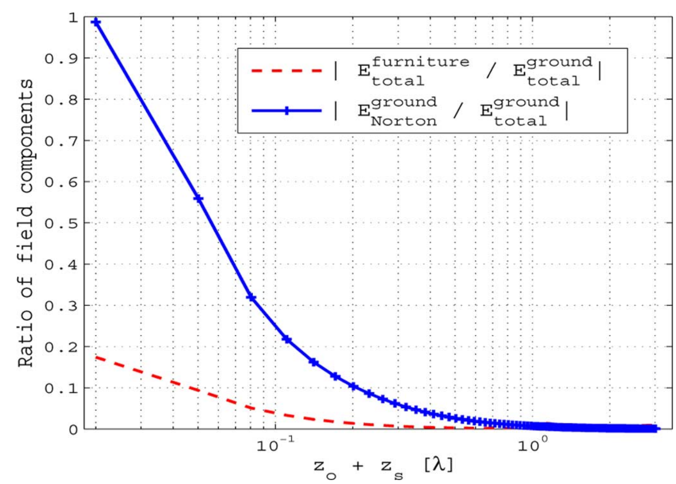

Fig. 7. Comparison of the effect of Norton waves and scattering from a furniture (a table). The dielectric constant of the ground was assumed to be $\epsilon_{rg} = 4 + j0.5995$ and that of the wooden furniture is $\epsilon_{rg} = 1.4 + j0.0728$. The simulation frequency is 300 MHz.

(table) is assumed to be the same as the total field in the absence of the table. The total field inside the wooden table is then used to calculate the volumetric polarization currents which are then used to predict the field component that is scattered by the table. This approximation is justified because the dielectric constant of the wooden table is relatively small. In addition, this approximation overestimates the exact total field inside the wooden table. Therefore, the scattered field calculated using this method will be an overestimation of the exact scattered electric field. If this estimate is much less than the Norton component, then we can confidently say that the exact field scattered by the table would also be much less than the Norton contribution. The ratio of the Norton component to the total received field is shown in Fig. 7 (solid curve). The dashed curve in Fig. 7 shows the ratio of the field scattered by the furniture to the total field received in the presence of the ground (without the furniture). The main point of this analysis is to show that, for near-ground transceivers, taking into account the Norton waves is much more important than the inclusion of scattering from furniture. So, by adding the Norton waves and utilizing physical and geometrical optics type approaches to take into account scattered field from relatively large indoor scatterers (building walls), we can significantly improve the accuracy of the predicted electric field compared to what the usual ray tracing approach provides. This comparison will be discussed in more detail later in this section.

C. Time-Domain Analysis of the Received Field

Analyzing the time domain characteristics of the technique is vital because it provides insight into the various scattering mechanisms. This knowledge can be applied to further refine the field prediction technique by focusing on the dominant contributions. In this analysis, the electric field for fixed source and observation points is computed in time-domain for a single wall-ground scenario like the one shown in Fig. 3 (with one wall). For this simulation, a vertical dipole positioned $10m$ away from the first wall is used as a Tx antenna and the observation point is $9.7\ \mathrm{m}$ away from the other side of the wall. The heights of the Tx and Rx antennas are $0.11\ \mathrm{m}$ and $0.1\ \mathrm{m}$, respectively. The wall extends from $x_w = 10\ \mathrm{m}$ to $x_w = 10.5\ \mathrm{m}$ and its height is 3 m. The dielectric constants of both the wall and the ground are chosen to be $\epsilon_r = 4.5 + 1.189j$. To calculate the time domain signal accurately, first the field at the observation point is computed as a function of frequency (at several frequency points). Then, the Inverse Fourier Transform is applied to the frequency domain field data. It should be noted that sufficient bandwidth and number of frequency points are needed to recover the time-domain signal accurately. The bandwidth dictates the spatial resolution in time-domain and the frequency step determines the time extent of the resulting time-domain signal. This means that if the bandwidth is too small, it won't be possible to differentiate the direct and diffracted components. Therefore, large bandwidth and very fine frequency step are needed. The frequency range used for this simulation is 5–405 MHz with 60 frequency points.

As shown in Fig. 8, two major peaks are found in the time domain plot of the received field. First, the actual distances (d_{act}) for both the direct and diffracted paths are calculated from the geometry used in the simulation and the estimated distances (d_{est}) for both paths are also calculated from the time delays of the peaks. Table I summarizes distances from the source to the receiver calculated based on the geometry and peak delays from the simulation for both the direct and diffracted signal paths. The first peak corresponds to the signal that is directly coupled between the transmitter and receiver through the wall in the presence of the ground. The second peak corresponds to the field diffracted by the top edge of the building wall. In both cases, there is a small error between the estimated and the actual distances (0.25% for the direct and 0.74% for the diffracted signals). This error is caused by the approximate calculation of the distances for both paths. This analysis is useful for applications where we want to separate the constituent components. For example, it becomes very useful when laboratory measurements are used for validation of the proposed technique to separate the multipath from the desired signal.

D. Semi-Analytic versus Full-Wave versus Ray Tracing

A multiwall scenario where an infinitesimal dipole located just above the ground and is radiating outside a room consisting of four walls is simulated based on the proposed semi-analytic technique. The same propagation scenario is also simulated using a commercial full-wave solver (FDTD based solver named Semcad X) and a ray tracing routine. This comparison serves two purposes. The Semcad X results validate the proposed technique while comparison with ray tracing shows the improvements that the new technique offers especially for near-ground propagation in indoor scenarios.

For this particular simulation, as can be seen in Fig. 4, the setup is as follows. The room is 3.9λ by 4.1λ and all four walls

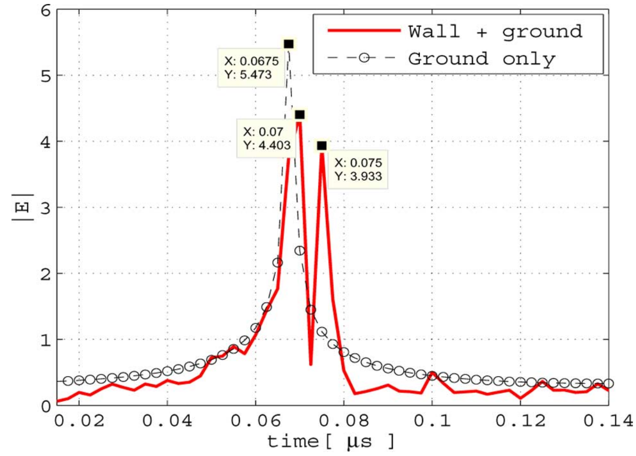

Fig. 8. Magnitude of the total electric field in time domain for a single wall-ground geometry as compared to the case where only the ground is considered.

TABLE I
COMPARISON OF THE PEAK DELAYS

	$d_{act}[m]$	$d_{est}[m]$	Physical mechanism
Peak 1	20.20	20.25	Direct signal with ground and wall
Peak 2	22.33	22.50	Diffracted by the top edge of the wall

have heights of 2.56λ and thickness 0.2λ. The Tx antenna is located 15λ away from the first wall and its height is 0.25λ. The electromagnetic properties used in this simulation for all the walls and the ground are $\epsilon_r = 4.5$ and $\sigma = 0.02$. The frequency used for this simulation is 300 MHz. It should be noted that the effects of doors, windows and other indoor obstacles are not included in this implementation, but these changes can be integrated in our model. The errors for both the semi-analytic (SA) and ray tracing (RT) techniques are calculated based on the following equation where E_{FW} represents the electric field computed based on the full-wave solver

$$\mathrm{error}_{RT,SA} = \frac{|E_{RT,SA} - E_{FW}|}{|E_{FW}|}. \tag{21}$$

The errors in the predicted electric field by the two methods are computed and plotted against position for the observation lines shown in Fig. 4 (Traces A and B). As can be seen in Fig. 9, the proposed approach has errors that are much lower than that of ray tracing. Of course, as the transceiver heights increase, the errors in the predicted electric fields by the two methods will be similar because the Norton waves become less significant at higher heights.

In addition, simulations showed that the proposed technique is more than five times faster than the full-wave solver. Similar to the 2D single wall case discussed, the discrepancies between the full-wave solution and that of the new technique is due to the various approximations made which are discussed in Section III-A. In addition, the approach used to include scattering from walls that are not in the line of sight of the Tx antenna (walls 2, 3, and 4 in Fig. 4) is essentially geometrical optics with the exception that the Norton waves are taken into account. This approximation also contributes to the discrepancies between the proposed method and the numerical result.

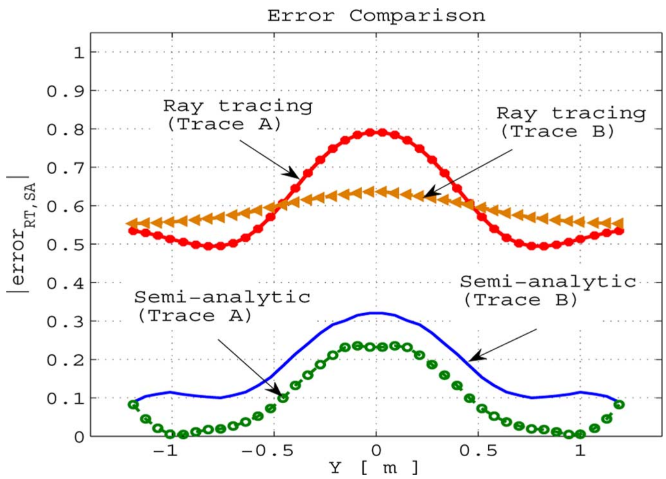

Fig. 9. The error introduced by using the semi-analytic method and ray tracing. For this simulation, a full-wave solver (Semcad X) is used as a reference. The observation lines (Traces A and B) are shown in Fig. 4.

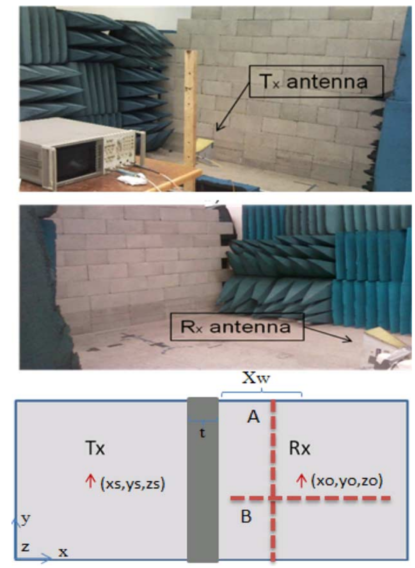

Fig. 10. Measurement setup consisting of concrete wall, network analyzer, Tx antenna (on one side of the wall) and Rx antenna (the other side of the wall). The dimensions of the wall are: $h = 1.56$ m, $L = 2.56$ m, and $t = 0.09$ m.

IV. Measurement Results

To further examine the validity of the proposed approach comparison against measurements under laboratory controlled environment is carried out. Controlled experiments under laboratory conditions are preferred over realistic settings as all the experimental parameters are well-characterized and features that can lead to uncertainty in the measurements can be suppressed or removed. As shown in Fig. 10, the experimental setup consists of a single wall build out of concrete blocks and two horn antennas used as Tx and Rx antennas positioned on either side of the wall. The length, height and thickness of the wall are 2.56, 1.56, and 0.09 m, respectively. The antennas are connected to the two channels of a network analyzer via long cables. The real part of the dielectric constant and the conductivity of concrete are assumed to be 4.5 and 0.02 S/m, respectively. The Tx antenna is positioned 1.74 m away from the wall. The received electric fields are recorded for various points by moving the receiver along traces A and B shown in Fig. 10. In the first case (a), the path is along the x axis where $y_s = 1.37$ m, $y_o = 1.37$ m, $z_s = 0.24$ m, and $z_o = 0.20$ m. In the second case (b), the trace is along the y axis for which $z_s = 0.24$ m, $x_w = 0.91$ m and $z_o = 0.20$ m. The final case (c) is the same as (b) but with different transceiver heights ($z_s = 0.87$ m and $z_o = 0.79$ m). Both the Tx and Rx antennas are oriented to provide vertical polarizations. The whole setup is surrounded by absorbers to minimize unwanted scattering from other objects in the laboratory.

For the setup described above, the ratio of the signal at the receiving channel of the network analyzer to the signal at the transmitting channel (S21) is measured from 1 to 5 GHz with 20 MHz frequency step. It should be noted that due to limitations imposed by the size of low frequency wideband antennas and the large size of the overall measurement setup (for low frequency measurements), we resorted to performing a scaled measurement at higher frequencies. The downside to using this method is that at these frequencies, the lowest antenna height (measured from the phase center) is limited by the size of the ultrawideband double-ridge horn antennas we used which are higher than the Tx and Rx antenna height values at which the Norton waves are dominant. However, since our method is still valid for any transceiver height, the scaled measurements can be used to demonstrate the accuracy of the proposed field prediction model compared to actual measurements. All measurements are performed first in the presence of the concrete wall. Then, a second set of measurements are performed without the wall to establish a reference for calibration.

The acquired field data needs to be calibrated before comparing it with results from the semi-analytic technique. As it was alluded to in Section III, the results from the time-domain analysis become helpful for calibration of the measured results. The goal is to remove unwanted multiple reflections from other scatterers in the laboratory since isolating the effect of the wall on the received field is what we want to achieve. Based on the conclusions drawn from the analysis in Section III-C, the dominant components for a single wall-ground set up are isolated in the measurement results. First the frequency domain data is converted to time domain by taking its inverse Fourier transform. Then, time-domain gating is performed by which components of the signal that are from unwanted scatterers are removed and the Fourier Transform is applied to the gated signal to obtain the frequency domain response of the transmission through the wall (E_{ww}). The same procedure is applied to the signal measured without the wall (E_{nw}). Finally, the resulting data is calibrated by dividing the transmission measurement obtained with the wall by that obtained without the wall.

The comparisons between the proposed approach and the measurements are shown in Fig. 11 where good agreements are demonstrated with about 10% error in all three cases. The cause of the discrepancies include the following: 1) the dielectric constants used in the simulation for the ground and the wall are only approximate values; 2) both the ground and the concrete wall have inhomogeneities and hence the effective dielectric properties already include errors; and 3) errors in the

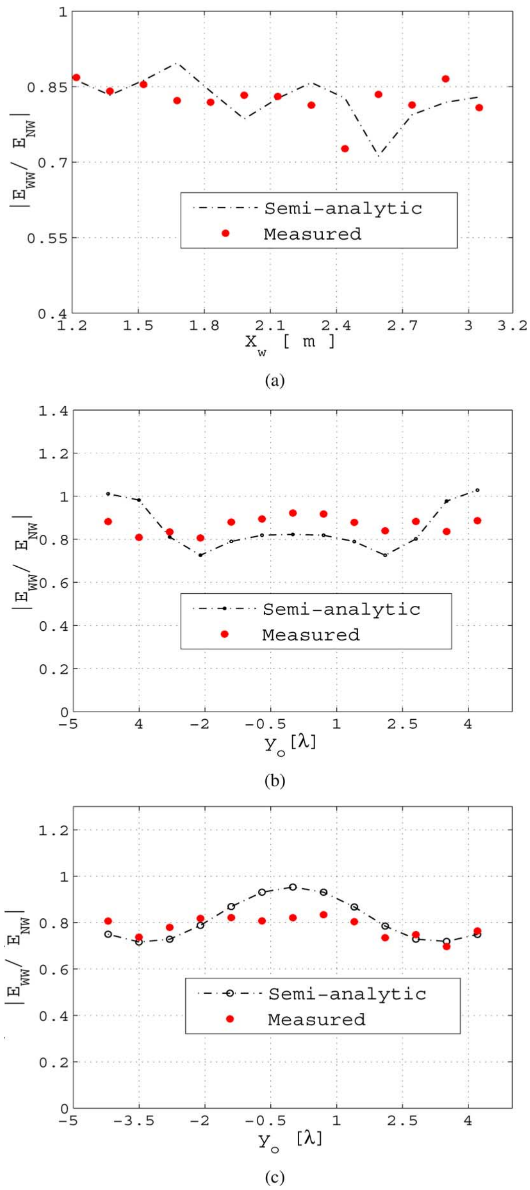

Fig. 11. Field magnitude comparison between the proposed semi-analytic method and measured values.

actual versus measured positions of the Tx and Rx antennas all contribute to the overall discrepancies seen in Fig. 11.

V. Conclusion

An efficient semi-analytic field prediction model for near-ground wave propagation in the presence of building walls is proposed. The method is based on a hybrid physical optics and asymptotic expansion of the dyadic Green's function for a half-space dielectric medium. Higher-order Norton surface waves which are typically neglected in more common indoor propagation techniques such as ray tracing are fully accounted for in this method as they prove to be vital for the accurate prediction of electric fields especially for transceivers that are less than a wavelength above the ground. To handle scattered field components from building walls in the presence of the ground, volume equivalence principle in conjunction with physical optics approximations is used. The formulation of the method for a single wall-ground geometry is presented followed by the approach we pursued to take into account multipath effects in realistic indoor environments which consist of multiple building walls and other indoor scatterers. A time-domain analysis for the single wall-ground geometry is also performed to get an insight into the various scattering mechanisms. The proposed method was validated by using numerical solvers as well as laboratory measurements. To show the significance of the Norton surface waves for near-ground transceivers, comparison of the scattered field component by a furniture against the contribution of Norton waves to the total electric field is presented. The performance of the proposed semi-analytic technique and the improvements it offers as compared to ray tracing is also discussed. For all the comparisons presented the observed errors and their explanations have been pointed out. Simulation results show that this method gives much more accurate results than ray tracing and proves to be computationally more efficient than a numerical method and therefore could be used to analyze field propagation for indoor scenarios that are large in terms of wavelength.

Appendix
Functions Used for Calculation of $\overline{\overline{G}}_{00}$

In this section, the expressions for $f_{ij}(w)$ used to compute the various components of the scattered field from a half-space dielectric are given by

$$E_{ij}^{scat} \simeq \frac{-k_o^3\eta_o I_o l_i}{8\pi} e^{ik_o\rho}\left[\frac{f_{ij}(w_s)}{ik_o\rho} + \frac{\frac{f''_{ij}(w_s)}{2} + \frac{f_{ij}(w_s)}{8}}{(ik_o\rho)^2}\right] \quad \text{(A.1)}$$

where

$$f_{xx}(w) = (\sin w)^{1/2}\cos w[R_-(w) - R_+(w)\cos(2\phi)] \quad \text{(A.2)}$$

$$f_{xy,yx}(w) = -(\sin w)^{1/2}\cos w R_+(w)\sin(2\phi) \quad \text{(A.3)}$$

$$f_{xz}(w) = \frac{2}{k_o}(\sin w)^{3/2}\cos w R_{TM}^{01}(w)\cos\phi \quad \text{(A.4)}$$

$$f_{yy}(w) = (\sin w)^{1/2}\cos w[R_-(w) + R_+(w)\cos(2\phi)] \quad \text{(A.5)}$$

$$f_{yz}(w) = \frac{2}{k_o}(\sin w)^{3/2}\cos w R_{TM}^{01}(w)\sin\phi \quad \text{(A.6)}$$

$$f_{zx}(w) = -\frac{2}{k_o}(\sin w)^{3/2}\cos w R_{TM}^{01}(w)\cos\phi \quad \text{(A.7)}$$

$$f_{zy}(w) = -\frac{2}{k_o}(\sin w)^{3/2}\cos w R_{TM}^{01}(w)\sin\phi \quad \text{(A.8)}$$

$$f_{zz}(w) = \frac{2}{k_o}(\sin w)^{5/2} R_{TM}^{01}(w). \quad \text{(A.9)}$$

The reflection coefficients $(R_{TE}, R_{TM}, R_\pm)$ are given

$$R_{TE}^{mn}(w) = \frac{\sqrt{\epsilon_{rm} - \sin^2 w} - \sqrt{\epsilon_{rn} - \sin^2 w}}{\sqrt{\epsilon_{rm} - \sin^2 w} + \sqrt{\epsilon_{rn} - \sin^2 w}} \quad \text{(A.10)}$$

$$R_{TE}^{mn}(w) = \frac{\epsilon_{rn}\sqrt{\epsilon_{rm} - \sin^2 w} - \epsilon_{rm}\sqrt{\epsilon_{rn} - \sin^2 w}}{\epsilon_{rn}\sqrt{\epsilon_{rm} - \sin^2 w} + \epsilon_{rm}\sqrt{\epsilon_{rn} - \sin^2 w}} \quad \text{(A.11)}$$

$$R_\pm(w) = \frac{R_{TE}^{01}(w)}{k_o\cos w} \pm \frac{\cos w R_{TM}^{01}(w)}{k_o} \quad \text{(A.12)}$$

REFERENCES

[1] M. Dehmollaian and K. Sarabandi, "Refocusing through building walls using synthetic aperture radar," *IEEE Trans. Geosci. Remote Sens.*, vol. 46, no. 6, Jun. 2004.

[2] M. Thiel and K. Sarabandi, "Analysis of human backscattering in buildings for through-wall radar applications," in *Proc. IEEE Antennas Propag. Soc. Int. Symp.*, Jun. 2009.

[3] [Online]. Available: http://www.globalsecurity.org/military/systems/munitions/shm.htm

[4] [Online]. Available: http://www.darpa.mil/ipto/programs/nest/nest.asp

[5] W. M. Merrill, H. L. N. Liu, J. Leong, K. Sohrabi, and G. J. Pottie, "Quantifying short-range surface-to-surface communications links," *IEEE Antennas Propag. Mag.*, vol. 46, no. 3, Jun. 2004.

[6] J. W. McKown and R. L. Hamilton Jr., "Ray tracing as a design tool for radio networks," *IEEE Netw. Mag.*, vol. 5, no. 6, Nov. 1991.

[7] R. A. Valenzuela, "A ray tracing approach to predicting indoor wireless transmission," *IEEE Trans. Veh. Technol.*, May 1993.

[8] F. Aryanfar and K. Sarabandi, "3-D wave propagation simulation in complex indoor structures," in *Proc. IEEE Antennas Propag. Soc. Int. Symp.*, Jun. 2004.

[9] M. Hassan-Ali and K. Pahlavan, "A new statistical model for site-specific indoor radio propagation prediction based on geometric optics and geometric probability," *IEEE Trans. Wireless Commun.*, vol. 1, Jan. 2002.

[10] F. A. Alves, M. R. M. L. Albuquerque, S. G. Silva, and A. G. d'Assuno, "Using efficient ray tracing techniques to predict propagation losses in indoor environments," *Microw. Opt. Technol. Lett.*, vol. 49, no. 4, Apr. 2007.

[11] V. Ercerg, S. J. Fortune, J. Ling, A. J. Rustako Jr., and R. A. Valenzuela, "Comparisons of a computer-based propagation prediction tool with experimental data collected in urban microcellular environments," *IEEE J. Sel. Areas Commun.*, vol. 15, no. 4, pp. 677–684, May 1997.

[12] G. E. Athanasiadou, A. R. Nix, and J. P. McGeehan, "A microcellular ray tracing propagation model and evaluation of its narrow-band and wide-band predictions," *IEEE J. Sel. Areas Commun.*, vol. 18, no. 3, pp. 322–335, Mar. 2000.

[13] S. Loredo, L. Valle, and R. P. Torres, "Accuracy analysis of GO/UTD radio-channel modeling in indoor scenarios," *IEEE Antennas Propag. Mag.*, vol. 42, no. 5, pp. 37–51, Oct. 2001.

[14] Z. Zhang, R. K. Sorensen, Z. Yun, M. F. Iskander, and J. F. Harvey, "A ray tracing approach for indoor/outdoor propagation through window structures," *IEEE Trans. Antennas Propag.*, vol. 50, no. 5, May 2002.

[15] K. A. Remley, H. R. Anderson, and A. Weisshar, "Improving the accuracy of ray tracing techniques for indoor propagation modeling," *IEEE Trans. Veh. Technol.*, vol. 49, no. 6, Nov. 2000.

[16] F. S. de Adana, O. G. Blanco, I. G. Diego, J. P. Arriaga, and M. F. Cátedra, "Propagation model based on ray tracing for the design of personal communication systems in indoor environments," *IEEE Trans. Veh. Technol.*, vol. 49, no. 6, May 2000.

[17] M. Thiel and K. Sarabandi, "3D-Wave propagation analysis of indoor wireless channels utilizing hybrid methods," *IEEE Trans. Antennas Propag.*, vol. 57, no. 5, May 2009.

[18] R. Janaswamy, "Path loss predictions in the presence of buildings on flat terrain: A 3-D vector parabolic equation approach," *IEEE Trans. Antennas Propag.*, vol. 51, no. 8, May 2003.

[19] S. Y. Tan and H. S. Tan, "UTD propagation model in an urban street scene for microcellular communications," *IEEE Trans. Electromag. Compat.*, vol. 35, Nov. 1993.

[20] R. J. Luebbers, "Finite conductivity uniform GTD versus knife edge diffraction in prediction of propagation path loss," *IEEE Trans. Antennas Propag.*, vol. AP-32, pp. 70–76, Jan. 1984.

[21] R. G. Kouyoumjian and P. H. Pathak, "A uniform geometric theory of diffraction for an edge on a perfectly conducting surface," *Proc. IEEE*, vol. 62, Nov. 1974.

[22] T. B. Gibson and D. C. Jenn, "Prediction and measurement of wall insertion loss," *IEEE Trans. Antennas Propag.*, vol. 47, no. 1, Jan. 1999.

[23] F. Van Der Wijk, A. Kegel, and R. Prasad, "Assessment of a picocellular system using propagation measurements at 1.9 GHz for indoor wireless communications," *IEEE Trans. Veh. Technol.*, vol. 44, Feb. 1995.

[24] K.-W. Cheung, J. H.-M. Sau, and R. D. Murch, "A new empirical model for indoor propagation prediction," *IEEE Trans. Veh. Technol.*, vol. 47, no. 3, Aug. 1998.

[25] A. Hugine, H. I. Volos, J. Gaeddert, and R. M. Buehrer, "Measurement and characterization of the near-ground indoor ultra wideband channel," in *Proc. Wireless Commun. Netw. Conf.*, 2006.

[26] M. Hata, "Empirical formula for propagation loss in land mobile radio service," *IEEE Trans. Veh. Technol.*, vol. VT-29, no. 3, pp. 317–325, 1980.

[27] J. B. Andersen, T. 5. Rappaport, and S. Yoshida, "Propagation measurements and models for wireless communications channels," *IEEE Commun. Mag.*, Jan. 1995.

[28] Q. H. Spencer, B. D. Jeffs, M. A. Jensen, and A. L. Swindlehurst, "Modeling the statistical time and angle of arrival characteristics of an indoor multipath channel," *IEEE J. Sel. Areas Commun.*, vol. 18, no. 3, Mar. 2000.

[29] K. Sarabandi, M. D. Casciato, and I.-S. Koh, "Efficient calculation of the fields of a dipole radiating above an impedance surface," *IEEE Trans. Antennas Propag.*, vol. 50, no. 9, Sep. 2002.

[30] W. C. Chew and J. A. Kong, "Electromagnetic field of a dipole on a two-layer earth," *EM Geophys.*, vol. 46, no. 3, Mar. 1981.

[31] T. Tamir, "Radio wave propagation along mixed paths in forest environments," *IEEE Trans. Antennas Propag.*, vol. 25, no. 4, Jul. 1977.

[32] D. Liao and K. Sarabandi, "Near-earth wave propagation characteristics of electric dipole in presence of vegetation or snow layer," *IEEE Trans. Antennas Propag.*, vol. 53, no. 11, Nov. 2005.

[33] K. A. Michalski and J. R. Mosig, "Multilayered media Green's functions in integral equation formulations," *IEEE Trans. Antennas Propag.*, vol. 45, no. 3, Mar. 1997.

[34] K. A. Norton, "The calculation of ground-wave field intensity over a finitely conducting spherical earth," in *Proc. IRE*, Dec. 1941, pp. 23–39.

[35] J. R. Wait, "The ancient and modem history of EM ground-wave propagation," *IEEE Antennas Propag. Mag.*, vol. 40, no. 5, pp. 7–24, Oct. 1998.

[36] C.-F. Yang, C.-J. Ko, and B.-C. Wu, "A free space approach for extracting the equivalent dielectric constants of the walls in buildings," in *Proc. IEEE Antennas Propag. Soc. Int. Symp*, 1996, vol. 2.

[37] D. Peña, R. Feick, H. D. Hristov, and W. Grote, "Measurement and modeling of propagation losses in brick and concrete walls for the 900-MHz band," *IEEE Trans. Antennas Propag.*, vol. 51, no. 1, Jan. 2003.

[38] D. Liao and K. Sarabandi, "Simulation of near-ground long-distance radiowave propagation over terrain using Nyström method with phase extraction technique and FMM-acceleration," *IEEE Trans. Antennas Propag.*, vol. 57, no. 12, Dec. 2009.

[39] F. T. Dagefu and D.-H. L. K. Sarabandi, "An efficient model for near-ground wave propagation in the presence of building walls/indoor obstacles," in *Proc. IEEE Antennas Propag. Soc. Int. Symp.* , Jun. 2009.

[40] W. C. Chew, *Waves and Fields in Inhomogeneous Media*. New York: Van Nostrand Reinhold, 1990.

[41] A. K. Jin, *Electromagnetic Wave Theory*. New York: Wiley-Interscience, 1990.

[42] [Online]. Available: www.awe-communications.com

Fikadu T. Dagefu (S'07) received the B.S. degree in electrical engineering from the University of Texas at Austin, in 2007 and the M.S. degree in electrical engineering from the University of Michigan, Ann Arbor, in 2009, where he is currently working toward the Ph.D. degree.

He has been a Graduate Student Research Assistant with the Radiation Laboratory, University of Michigan, Ann Arbor, since January 2008. His research focus includes near-ground wave propagation in complex environments and subsurface imaging based on distributed near-ground sensor networks.

Mr. Dagefu is a member of Eta Kappa Nu and Tau Beta Pi honor societies. He was a finalist in the Student Paper competitions at the IEEE IGARSS International Conference both in 2009 and 2010.

Kamal Sarabandi (S'87–M'90–SM'92–F'00) received the B.S. degree in electrical engineering from Sharif University of Technology, Tehran, Iran, in 1980, and the M.S. degree in electrical engineering and the M.S. degree in mathematics, both in 1986, and the Ph.D. degree in electrical engineering in 1989, all from the University of Michigan at Ann Arbor.

He is currently the Director of the Radiation Laboratory and the Rufus S. Teesdale Professor of Engineering with the Department of Electrical Engineering and Computer Science, the University of Michigan at Ann Arbor. His research areas of interest include microwave and millimeter-wave radar remote sensing, meta-materials, electromagnetic wave propagation, and antenna miniaturization. He has 25 years of experience with wave propagation in random media, communication channel modeling, microwave sensors, and radar systems and leads a large research group including two research scientists and 14 Ph.D. students. He has graduated 36 Ph.D. and supervised numerous postdoctoral students. He has served as the Principal Investigator on many projects sponsored by the National Aeronautics and Space Administration (NASA), Jet Propulsion Laboratory (JPL), Army Research Office (ARO), Office of Naval Research (ONR), Army Research Laboratory (ARL), National Science Foundation (NSF), Defense Advanced Research Projects Agency (DARPA), and a large number of industries. Currently, he is leading the Center for Microelectronics and Sensors funded by the Army Research Laboratory under the Micro-Autonomous Systems and Technology (MAST) Collaborative Technology Alliance (CTA) program. He has published many book chapters and more than 185 papers in refereed journals on miniaturized and onchip antennas, meta-materials, electromagnetic scattering, wireless channel modeling, random media modeling, microwave measurement techniques, radar calibration, inverse scattering problems, and microwave sensors.

Dr. Sarabandi is a member of Commissions F and D of URSI. He served as a member of NASA Advisory Council appointed by the NASA Administrator for two consecutive terms from 2006 to 2010. He is serving as a Vice President of the IEEE Geoscience and Remote Sensing Society (GRSS) and is a member of the Editorial Board of the IEEE PROCEEDINGS. He was an Associate Editor of the IEEE TRANSACTIONS ON ANTENNAS AND PROPAGATION and the IEEE SENSORS JOURNAL. He was the recipient of the Henry Russel Award from the Regent of The University of Michigan. In 1999, he received a GAAC Distinguished Lecturer Award from the German Federal Ministry for Education, Science, and Technology. He was also a recipient of the 1996 EECS Department Teaching Excellence Award and a 2004 College of Engineering Research Excellence Award. In 2005 he received the IEEE GRSS Distinguished Achievement Award and the University of Michigan Faculty Recognition Award. He also received the Best Paper Award at the 2006 Army Science Conference. In 2008, he was awarded a Humboldt Research Award from The Alexander von Humboldt Foundation of Germany and received the Best Paper award at the IEEE Geoscience and Remote Sensing Symposium. He was also awarded the 2010 Distinguished Faculty Achievement Award from the University of Michigan. He has also had more than 442 papers and invited presentations in many national and international conferences and symposia on similar subjects. The IEEE Board of Directors announced him as the recipient of the 2011 IEEE Judith A. Resnik medal. In the past several years, joint papers presented by his students at a number of international symposia (IEEE APS'95,'97,'00,'01,'03,'05,'06,'07; IEEE IGARSS'99,'02,'07; IEEE IMS'01, USNC URSI'04,'05,'06,'10,'11 AMTA'06, URSI GA 2008) have received Best Paper awards.